

GAF: Gaussian Avatar Reconstruction from Monocular Videos via Multi-view Diffusion

Jiapeng Tang¹ Davide Davoli² Tobias Kirschstein¹ Liam Schoneveld³ Matthias Nießner¹

¹Technical University of Munich ²Toyota Motor Europe NV/SA ³Woven by Toyota
associated partner by contracted service

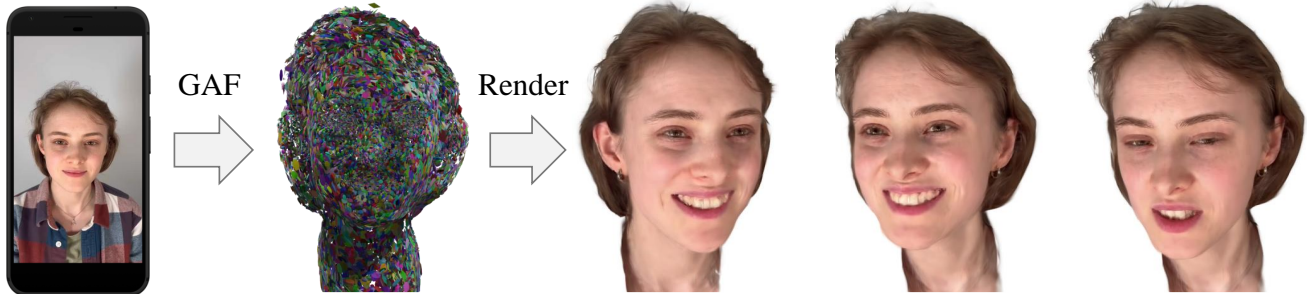


Figure 1. Given a short, monocular video captured by a commodity device such as a smartphone, GAF reconstructs a 3D Gaussian head avatar, which can be re-animated and rendered into photo-realistic novel views. Our key idea is to distill the reconstruction constraints from a multi-view head diffusion model in order to extrapolate to unobserved views and expressions.

Abstract

We propose a novel approach for reconstructing animatable 3D Gaussian avatars from monocular videos captured by commodity devices like smartphones. Photorealistic 3D head avatar reconstruction from such recordings is challenging due to limited observations, which leaves unobserved regions under-constrained and can lead to artifacts in novel views. To address this problem, we introduce a multi-view head diffusion model, leveraging its priors to fill in missing regions and ensure view consistency in Gaussian splatting renderings. To enable precise viewpoint control, we use normal maps rendered from FLAME-based head reconstruction, which provides pixel-aligned inductive biases. We also condition the diffusion model on VAE features extracted from the input image to preserve details of facial identity and appearance. For Gaussian avatar reconstruction, we distill multi-view diffusion priors by using iteratively denoised images as pseudo-ground truths, effectively mitigating over-saturation issues. To further improve photorealism, we apply latent upsampling to refine the denoised latent before decoding it into an image. We evaluate our method on the NeRSemble dataset, showing that GAF outperforms the previous state-of-the-art methods in novel view synthesis by a 5.34% higher SSIM score. Furthermore, we demonstrate higher-fidelity avatar reconstructions from monocular videos captured on commodity devices. [Project Page: https://tangjiapeng.github.io/projects/GAF](https://tangjiapeng.github.io/projects/GAF)

1. Introduction

Creating photorealistic and animatable head avatars has long been a challenge in computer vision and graphics. This is crucial for a vast variety of applications such as immersive telepresence in virtual and augmented reality, computer games, movie effects, virtual classrooms, and videoconferencing. Here, the goal is to generate avatars that can be realistically rendered from any viewpoint, accurately capturing facial geometry and appearance, while also enabling easy animation for realistic head portrait videos depicting various expressions and poses. The democratization of high-fidelity head avatars from commodity devices is a challenge of widespread interest. However, photo-realistic head avatar reconstruction from monocular videos is challenging and ill-posed, due to limited head observations causing a lack of constraints for novel-view rendering.

To create photorealistic, animatable human avatars, researchers have integrated NeRF [41, 42] and Gaussian Splatting (GS) [22] techniques with parametric head models [16, 30, 64], enhancing control over unseen poses and expressions. Approaches like [17, 48, 76, 77] achieve high-quality head reconstructions and realistic animations using dense multi-view datasets, typically captured in controlled studio settings. However, these methods encounter significant limitations with monocular recordings from commodity cameras, such as smartphone portrait videos. Monocular methods [1, 8, 14, 57, 75, 87, 88, 91] aim to reconstruct head avatars from single-camera videos but often rely on

substantial head rotations to capture various angles. They only reconstruct visible regions from input frames, leaving occluded areas incomplete and under-constrained. For instance, as illustrated in Fig. 4, front-facing videos provide limited capture on side regions, leading to visible artifacts when rendering extreme side views.

To this end, we introduce a multi-view head diffusion model that learns the joint distribution of multi-view head images. Given a single-view input image, our model generates a set of view-consistent output images. By leveraging view-consistent diffusion priors on human heads, our approach enables the robust reconstruction of Gaussian avatars, preserving both appearance and identity across novel perspectives. Unlike existing methods [34, 59, 71, 73] that use camera pose as a conditioning factor for viewpoint control, we use the normal map rendered from a reconstructed parametric face model as guidance. The normal maps provide stronger inductive biases, offering more precise and reliable novel view generation for heads. Specifically, we condition our multi-view diffusion process on 2D features extracted from the input image’s autoencoder, rather than only using high-level semantic vectors like CLIP embeddings [49]. This design allows us to incorporate fine-grained identity and appearance details directly into the multi-view denoising process, ensuring that the generated images maintain coherence and consistency across viewpoints in terms of identity and appearance.

In order to exploit multi-view diffusion priors for Gaussian head reconstruction, we employ a diffusion loss that uses iteratively denoised images as pseudo-ground truths for novel view renderings, instead of using a single-step score distillation sampling loss [45]. Moreover, to improve the fidelity of the Gaussian renderings, we introduce a latent upsampler model to enhance facial details within the denoised latent before decoding it back to image space. As demonstrated in Fig. 1, our approach generates high-quality, photorealistic novel views of head avatars using only short monocular videos captured by a smartphone. Extensive comparisons with state-of-the-art methods show that our approach delivers higher fidelity and more view-consistent avatar reconstructions from monocular videos. Our GAF significantly outperforms state-of-the-art methods, achieving 5.34% higher SSIM in novel view synthesis on the NeRSemble dataset.

Our contributions can be summarized as follows:

- We introduce a novel approach for reconstructing photorealistic, animatable head avatars from monocular videos with limited coverage captured on commodity devices, using multi-view head diffusion priors to regularize and complete unobserved regions.
- We propose a multi-view head diffusion model that generates consistent multi-view images from a single-view input, guided by normal maps rendered from FLAME head

reconstructions to improve viewpoint control.

- We present a mechanism for enhancing the photorealism and cross-view consistency of Gaussian splatting by integrating latent upsampling and multi-view diffusion priors.

2. Related Work

3D Scene Representations. Neural radiance fields [41] and its variants [2–4, 7, 9, 13, 42] revolutionized 3D scene reconstruction from multi-view images. However, NeRF-based methods are often hindered by computational inefficiency during both training and inference stages. Gaussian Splatting [22] represents a scene as a composition of discrete geometric primitives, *i.e.* 3D Gaussians, and employs an explicit rasterizer for rendering. Compared to NeRF, GS has achieved notable runtime speedups in the training and inference stages. This enables real-time performance and more favorable image synthesis. Unlike polygonal meshes, which require careful topology handling, GS supports substantial topology changes, making it more adaptable to complex surfaces and varying densities.

Parametric Face/Head Models. Based on statistical priors of 3D morphable models (3DMM)[5, 19, 30, 68, 70], many works [12, 18, 23, 67] learn 3D face/head reconstruction and tracking from single RGB images/videos. More recent methods [16, 64, 85, 87] leveraged signed distance fields [44] and deformation fields [43, 61, 62] based on coordinate-MLPs for more fine-grained geometry reconstruction including hair and beards. HeadGAP [86] and GPHM [78] learned parametric models for head Gaussians. Our work uses the VHAP tracker [47] to obtain coarse geometries as guidance for dynamic avatar reconstruction.

Photo-realistic Avatar Reconstruction. To create photo-realistic animatable head avatars, several works [14, 48, 57, 75, 76, 91] have combined NeRF/GS with 3D morphable models (3DMM). NerFace [14] learned expression-dependent NeRF using head parameters from monocular videos. INSTA [91] and H3QAvatar [66] mapped query points to a canonical space via deformation fields and defined multi-resolution hash grids for head radiance fields. PointAvatar [88] explored point-based representations for efficient training. Our work is closely related to animatable Gaussian splats [48, 57], which attached splats to the triangles of a FLAME mesh, and updated their properties by triangle deformations controlled by FLAME parameters. Although promising results have been achieved, they typically require multi-view setups with high-quality cameras in studio environments [27, 36]. Some works reconstruct avatars from monocular videos [1, 75, 88, 91]. However, they only reconstruct the visible region from inputs, lacking effective priors to complete missing areas. To address this, we utilize multi-view diffusion priors to complete unobserved regions of the face, ensuring photorealistic renderings from

extremely hold-out viewpoints.

Distillation 2D Priors for 3D Generation. Researchers have demonstrated that large-scale pretrained text-to-image priors [51, 52, 55] can be distilled for 3D asset generation [31, 63] using the score distillation sampling (SDS) loss proposed by DreamFusion [45] and its variants [39, 72, 81]. Several studies [6, 20, 90] applied SDS loss for text-driven 3D head avatar generation. For single-view 3D reconstruction, approaches like RelFusion [39], Magic123 [46], and Dreambooth3D [50] adapt text-to-image diffusion priors to specific objects to preserve identity. However, achieving consistent novel views from text prompts alone remains challenging without leveraging the input image. To address this, we choose to learn multi-view image diffusion priors conditioned on a single image. Rather than using a single-step SDS loss, we use iteratively denoised images as pseudo-ground truths for novel view supervision, similar to ReconFusion [74]. By integrating latent upsampler diffusion with joint multi-view latent denoising, we enhance both multi-view consistency and fidelity.

Multi-view Diffusion Models. Instead of text-to-image diffusion priors, some works learn image-conditioned novel view diffusion priors, which leverage the identity and appearance details of the input image to generate consistent novel views. 3DiM [73] pioneered a diffusion model for pose-conditioned novel view generation. Zero-123 fine-tune StableDiffusion [52] on Objaverse [10, 11] dataset to improve generalization ability. Some works learn to generate consistent multiple views from a single image via introducing dense 3D self-attention or epipolar attention in the denoiser network, including MVDiffusion [65], SyncDreamer [35], Zero-123++ [58], Wonder3D [37], MVDream [59], ImageDream [71], Human3Diffusion [79], IM3D [40], CAT3D [15], and VideoMV [92]. These works primarily target general objects, whereas our focus is specifically on human heads. To obtain more specialized priors, we train multi-view diffusion models on a dedicated multi-view head video dataset. By using normal maps from FLAME mesh reconstruction as the camera condition, we achieve precise viewpoint control for head rendering. This pixel-aligned inductive bias introduced by normal maps enables more accurate novel view synthesis, crucial for consistent head Gaussian supervision.

3. Preliminaries

3.1. 3D Gaussian Splatting

3D Gaussian Splatting [22] parameterizes a scene using a set of discrete geometric primitives known as 3D Gaussian splats. Each splat is characterized by a covariance matrix Σ centered at location μ . The covariance matrices are required to be semi-definite for physical interpretations. It utilizes a parametric ellipsoid definition to construct the covariance

matrix $\Sigma = RSS^T R^T$ using a scaling matrix S and a rotation matrix R . These matrices are independently optimized and represented by a scaling vector $\mathbf{s} \in \mathbb{R}^3$ and a quaternion $\mathbf{q} \in \mathbb{R}^4$. $\mathbf{r} \in \mathbb{R}^{3 \times 3}$ denotes the corresponding rotation matrix of \mathbf{q} . To represent scene appearance, sphere harmonic coefficients are used to represent the color \mathbf{c} of each Gaussian. During rendering, a tile-based rasterizer is used to α -blend all 3D Gaussians overlapping the pixel within a tile. To respect visibility order and avoid per-pixel sorting expenses, splats are sorted based on depth values within each tile before blending.

3.2. Gaussian Avatars

To animate Gaussian splats for head avatars, we use the representation of GaussianAvatars [48] to rig 3D Gaussians using the FLAME mesh. Initially, they bind each triangle of the FLAME identity mesh with a 3D Gaussian and transform the 3D Gaussian based on triangle deformations across different time steps. The splat remains static in the local space of the attached triangle but can dynamically evolve in the global metric space along rotation, translation, and scaling transformations of the binding triangle. For each triangle, they compute the mean position \mathbf{T} of its three vertices coordinates as the origin of the local space. They define a rotation matrix \mathbf{R} to depict the orientation of the triangle in the global space, composed of three column vectors derived from the direction vector of one edge, the normal vector of the triangle face, and their cross product. Additionally, they determine triangle scaling k by calculating the mean length of one edge and its perpendicular in a triangle. The 3D Gaussian is parameterized by the location μ , rotation \mathbf{r} , and anisotropic scaling \mathbf{s} in the local space of its parent triangle. In the initialization stage, the location μ is set as zero, rotation \mathbf{r} as an identity matrix, and scaling \mathbf{s} as a unit vector. During rendering, they transform these properties from local to global space by:

$$\mathbf{r}' = \mathbf{R}\mathbf{r} \quad (1)$$

$$\mu' = k\mathbf{R}\mu + \mathbf{T} \quad (2)$$

$$\mathbf{s}' = k\mathbf{s} \quad (3)$$

To capture fine-grained details in the rendered output, an adaptive density control strategy dynamically creates new Gaussians for each triangle based on screen-space positional gradients. This densification process operates within local space, where newly added Gaussians inherit binding relations from their original counterparts.

4. Gaussian Avatars Fusion

Given a monocular sequence of RGB images $\mathcal{I} = \{\mathbf{I}_i\}$ as input, our goal is to reconstruct head Gaussian splats $\mathcal{O} = \{\mathcal{O}_i\}$ as output. The overall pipeline is shown in

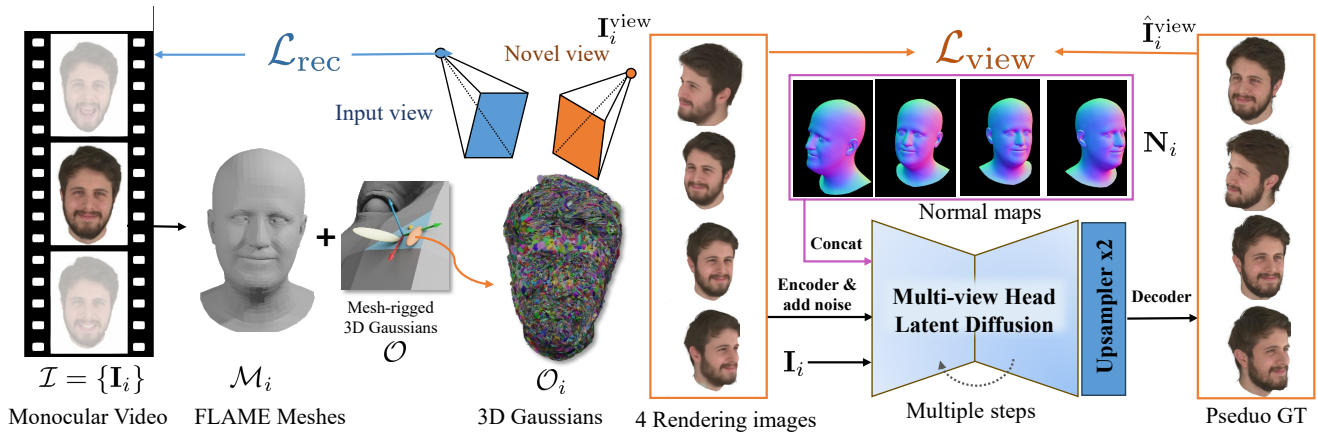


Figure 2. **Pipeline overview.** Given a sequence of RGB images from monocular cameras $\mathcal{I} = \{\mathbf{I}_i\}$, our objective is to reconstruct dynamic head avatars by optimizing an animatable Gaussian splatting representation \mathcal{O} , which is deformed to each frame as \mathcal{O}_i by the tracked FLAME mesh \mathcal{M}_i of \mathbf{I}_i . We optimize \mathcal{O} by minimizing an input view reconstruction loss \mathcal{L}_{rec} , plus a view sampling loss $\mathcal{L}_{\text{view}}$. $\mathcal{L}_{\text{view}}$ compares novel-view renderings of \mathcal{O}_i from four random viewpoints $\mathbf{I}_i^{\text{view}}$, with pseudo ground truths $\hat{\mathbf{I}}_i^{\text{view}}$, predicted by a multi-view head latent diffusion model. $\hat{\mathbf{I}}_i^{\text{view}}$ are generated by iteratively denoising 4-view latents, guided by the input image \mathbf{I}_i and normal maps \mathbf{N}_i rendered from \mathcal{M}_i . A latent upsampler module enhances facial details before decoding the denoised latent into an RGB image.

Figure 2. To enable animation of the reconstructed avatar with various head poses and expressions, we optimize the Gaussian splats \mathcal{O} rigged by a parametric head model, *e.g.* FLAME. The challenge is that monocular videos often lack complete observations of the head. For example, a front-facing video with limited head rotations may provide insufficient information about the face’s sides. This poses difficulties for reconstructing a photorealistic 3D head from partial input, as the optimization over \mathcal{O} is underconstrained. To address this, we introduce a normal map-guided, multi-view head diffusion model, which is designed to jointly denoise multi-view images conditioned on a single input image and normal maps rendered from FLAME tracking. Once trained, this model serves as a prior to regularize renderings from \mathcal{O} , filling in unobserved regions and improving the quality of the reconstructed avatar.

4.1. Normal map-conditioned Multi-view Head Latent Diffusion

To address missing regions in monocular videos with limited head coverage, one solution is to distill pre-trained text-to-image diffusion models to regularize novel view renderings. Personalized techniques like Dreambooth [54] allow for identity preservation by customizing diffusion models for specific objects we wish to reconstruct. However, since monocular videos may lack comprehensive side-view coverage, these models are prone to view bias: generated images tend to default to front-view perspectives, making it challenging to produce plausible novel views. Nevertheless, personalized text-to-image diffusion models are not designed to capture the distribution of novel views from a single input image. To overcome this, we propose a novel view diffusion model that generates identity-preserved and appearance-coherent novel views conditioned on an input

image. By denoising multiple novel views simultaneously, our approach enhances cross-view consistency. The multi-view head diffusion model is illustrated in Fig. 3.

Normal Map Conditioning. To control viewpoint, we leverage normal maps rendered from the FLAME mesh reconstruction at target views as diffusion guidance. The normal map is first encoded into a latent representation via pre-trained VAE [25], matching the dimensionality of the noisy image latent, and these two latents are then concatenated along the channel dimension. Compared to camera pose embeddings, normal maps offer a more explicit inductive bias for view synthesis by providing pixel-aligned conditioning, which facilitates alignment between the generated images and the conditioning normal maps. Moreover, the FLAME renderings also facilitate the expression accuracy of synthesized novel views.

Model Architecture. We train a multi-view diffusion model that takes a single image of a head, \mathbf{I}_{cond} , as input and generates multiple output images conditioned on normal maps rendered from desired camera poses using the FLAME reconstruction \mathcal{M} . Specifically, given \mathbf{I}_{cond} and the FLAME mesh \mathcal{M} , the model learns the joint distribution of N target images, \mathbf{I}_{tgt} , guided by N normal maps, \mathbf{N}_{tgt} , which are rendered from \mathcal{M} at the target camera poses.

$$p(\mathbf{I}_{\text{tgt}}|\mathbf{I}_{\text{cond}}, \mathbf{N}_{\text{tgt}}) \quad (4)$$

Our model architecture is similar to multi-view diffusion models (MVLDM) [15, 59, 71, 79], which is based on 2D U-Net [53] and attention blocks [69]. As shown in Fig. 3, we use the CLIP image embedding to achieve global control over novel view generation. However, this embedding mainly contains high-level semantic features, lacking the detailed information necessary for accurately capturing the

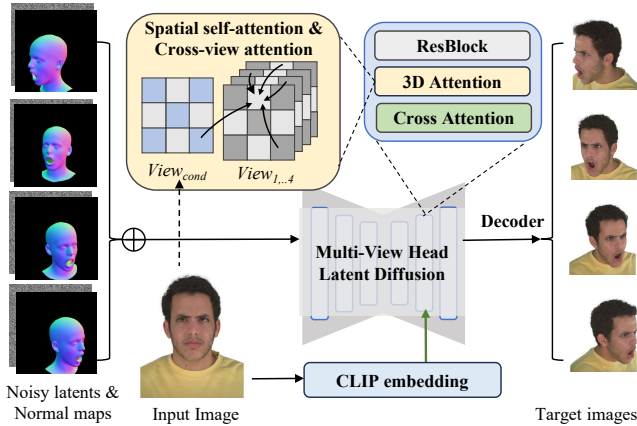


Figure 3. **Multi-view latent head diffusion models.** Given multi-view noisy image latents, we concatenate them with VAE latents of normal maps rendered from FLAME tracking. These combined inputs are processed by a 2D U-Net denoiser with attention blocks. To maintain 3D consistency, 3D attention blocks apply cross-attention across all views, integrating face identity and appearance details from the input image into the denoised latents while allowing information exchange between noisy latents across views. Additionally, the CLIP embedding of the input image is used for global control via cross-attention blocks.

head’s identity and appearance. To address this, we incorporate the VAE latents of \mathbf{I}_{cond} directly into the multi-view diffusion model. By applying cross-attention between the multi-view denoised latents and the VAE latent of \mathbf{I}_{cond} , we effectively transfer identity-specific details. Additionally, to ensure consistency across views, we aggregate information from the noisy latents across different viewpoints.

4.2. Gaussian Avatars Reconstruction with Multi-view Diffusion Priors

We now seek to utilize the multi-view diffusion priors for head Gaussian reconstruction. A commonly used strategy is Score Distillation Sampling (SDS) loss [45]. Let us denote the rendered image from Gaussian as \mathbf{x} . One can add noise ϵ at time step t to the input image \mathbf{x} to obtain a noisy image \mathbf{x}_t , which is fed into denoising network to estimate out the noise $\hat{\epsilon}$. The SDS loss calculates the difference $\|\hat{\epsilon} - \epsilon\|_2^2$. The gradients can be back-propagated to update 3D representation. The SDS loss essentially performs one-step denoising. Due to the stochastic nature of the denoising process introduced by random noise levels and seeds, it contains noisy gradients that disturb 3D optimization. Consequently, it often causes over-saturated appearance issues in synthesized 3D assets. Wu et al. [74] found that after iteratively denoising \mathbf{x}_t for multiple steps, we can obtain a deterministic output \mathbf{x}_0 . Based on this observation, we can calculate $\|\mathbf{x}_0 - \mathbf{x}\|_2^2$ as the diffusion loss for 3D Gaussian optimization.

Pseudo-image Ground Truths. At each iteration, we randomly select the i -th input frame \mathbf{I}_i and its FLAME mesh \mathcal{M}_i . By randomly sampling 4 viewpoints $\{\phi_j\}_{j=1}^4$,

then we can generate 4 random novel views from $\mathbf{I}_i^{view} = \mathcal{R}(\mathcal{O}_i, \{\phi_j\})$, and render normal maps $\mathbf{N}_i = \mathcal{R}(\mathcal{M}_i, \{\phi_j\})$ from \mathcal{M}_i . We can employ normal map-guided multi-view diffusion priors to regularize \mathbf{I}_i^{view} . Concretely, we encode \mathbf{I}_i^{view} into latent features \mathbf{z} , which is perturbed with noise ϵ_t to obtain noisy feature \mathbf{z}_t . The noise intensity of ϵ_t is controlled by the diffusion time step $t \sim [0.02, 0.98]$. We then iteratively perform multiple denoising steps of latent diffusion until the final clean latent \mathbf{z}_0 is obtained. To accelerate the generation speed, we adopt the DDIM sampling strategy [60] by running t/k intermediate steps, which can reduce the denoising steps by $k = 20$ times. Then \mathbf{z}_0 is decoded back to 4 images $\hat{\mathbf{I}}_i^j$ that can be served as pseudo supervision.

Latent Upsampler. To further enhance the facial details in $\hat{\mathbf{I}}_i^{view}$, we use a latent upsampler diffusion model to super-resolve the denoised 4-view latents \mathbf{z}_0 , from a resolution of 32×32 to 64×64 . This super-resolution step allows the pseudo-image ground truths $\hat{\mathbf{I}}_i^j$ to reach a final resolution of 512×512 . We use 10-step DDIM sampling in our latent upsampler inference.

3D-Aware Denoising. The rendered views \mathbf{I}_i^{view} from a global 3D representation \mathbf{O}_i introduce 3D-awareness into the denoising process, further enhancing multi-view consistency across pseudo ground truths $\hat{\mathbf{I}}_i^j$.

4.3. Loss Functions

We supervised the optimization of Gaussian Splats \mathcal{O} by a combination of loss functions in the following:

$$\mathcal{L} = \mathcal{L}_{img}(\mathbf{I}^{rec}, \mathbf{I}) + L_{img}(\mathbf{I}^{view}, \hat{\mathbf{I}}^{view}) + \lambda_{pos} \mathcal{L}_{pos} + \lambda_{scale} \mathcal{L}_{scale} \quad (5)$$

L_{img} is defined by a combination of pixel-wise L_1 loss, SSIM loss, and LPIPS loss:

$$\mathcal{L}_{img} = \lambda_1 \mathcal{L}_1 + \lambda_2 \mathcal{L}_{SSIM} + \lambda_3 \mathcal{L}_{LPIPS} \quad (6)$$

where $\lambda_1 = 0.8$, $\lambda_2 = 0.2$, and $\lambda_3 = 0.1$. We also introduce splat position and scale regularization terms to penalize abnormally distributed splats. The position regularization term ensures that Gaussians remain close to their attached triangles during optimization through:

$$\mathcal{L}_{pos} = \|\max(\mu, \epsilon_{pos})\|_2 \quad (7)$$

where $\epsilon_{pos} = 1$ serves as the threshold, allowing small positional errors within the scaling of the attached triangle. The scale regularization term mitigates the formation of large Gaussians, which could lead to jittering problems due to small rotations of triangles.

$$\mathcal{L}_{scale} = \|\max(\mathbf{s}, \epsilon_{scale})\|_2 \quad (8)$$

It will be disabled when the local scale of the Gaussian w.r.t the attached triangle is less than $\epsilon_{pos} = 0.6$. λ_{pos} and λ_{scale} are set to 0.01 and 1 respectively.

4.4. Implementation Details

Multi-view Head Diffusion Model. It is initialized from Stable Diffusion 2.1 [52] of ImageDream [71] and is trained on eight A100 GPUs over 20,000 iterations, taking approximately 72 hours. The training uses a learning rate of 0.0001 and a batch size of 64. During training, we employ a classifier-free guidance strategy, randomly dropping the input image at a rate of 0.1. The model is trained on the multi-view human head video dataset NeRSemble [27], which contains RGB video sequences from 16 viewpoints, covering both front and side faces. We randomly sample 50,000 timesteps to construct the training dataset.

Gaussian Avatar Optimization. The FLAME meshes are initially obtained by VHAP tracker [47] from monocular videos. The animatable Gaussians are optimized with Adam [26] for 6,000 iterations, with learning rates of $5e-5$, $1.7e-2$, $1e-3$, $2.5e-3$, and $5e-2$ for splat position, scaling factor, rotation quaternion, color and opacity respectively. We perform adaptive densification if the position gradients are larger than 0.0002 in every 300 iterations until 5,000 iterations are reached. We also remove Gaussians with opacity less than 0.005. During training, we also fine-tune the FLAME parameters using the learning rates $1e-6$, $1e-5$, and $1e-3$ for translation, joint rotation, and expression coefficients. We randomly sample 4 novel viewpoints to calculate multi-view diffusion loss. The azimuth range is $[-90^\circ, 90^\circ]$, the elevation range is $[-30^\circ, 30^\circ]$, and the distance between the camera and the head avatar location is between 1.0 and 1.2 units.

Runtime. Our current implementation of avatar reconstruction takes about 12 hours and uses 32 GB of memory on a single A6000 GPU. After avatar reconstruction, our method takes 0.0026 seconds to render an image at 768×768 resolution, i.e. 384.3fps.

5. Experiments

Datasets. We conduct head avatar reconstruction experiments on monocular video sequences from the **NeRSemble dataset** [27]. Note that these evaluation sequences were not seen by the multi-view diffusion model. We use monocular videos from the 8-th camera as the input, only capturing the head from the front view. And we use videos from the other 15 views for evaluation. We randomly select 12 sequences from different identities, with durations between 70 and 300 frames, downsampled to a resolution of 802×550 . Additionally, we include a **Monocular Video** dataset consisting of 3 monocular videos from the INSTA [91] dataset at 512×512 resolution, and 3 sequences of three subjects captured by smartphone at 1280×720 resolution.

Evaluations. Following previous works [48, 91], we report the average L1 loss, LIPIS, PSNR, and SSIM between ren-

Method	Novel Views			Novel Expressions		
	LPIPS ↓	PSNR ↑	SSIM ↑	LPIPS ↓	PSNR ↑	SSIM ↑
INSTA [91]	0.262	15.87	77.02	0.165	19.46	84.91
FlashAvatar [75]	0.247	16.94	81.05	0.145	21.37	86.08
GA [48]	0.218	17.51	81.66	0.138	21.63	87.00
Ours	0.158	19.20	87.00	0.111	22.78	89.46

Table 1. Quantitative comparisons on dynamic avatar reconstruction and animation from monocular videos. Results are obtained by the average of twelve sequences of different subjects on the **NeRSemble dataset**.

derings and ground truths of the test set. In the NeRSemble dataset, we evaluate head avatar reconstruction and animation quality in two settings: 1) *novel view synthesis*: driving a reconstructed avatar with seen head poses and expressions during training, and rendering it from 15 hold-out viewpoints. 2) *novel expression synthesis*: driving a reconstructed avatar with unseen head poses and expressions during training, and rendering it, rendered from 5 nearby hold-out views, i.e. cameras 6–10. For this dataset, 80% of frames are used for training, and 20% for evaluation. In the Monocular Video dataset, we use around 40% of frames for training and the rest for evaluation. The training sets consist of front-facing frames, while the evaluation set includes obvious head rotations to capture side faces.

Baselines. We compare our method against three state-of-the-art methods. *GaussianAvatars*[48] is designed to reconstruct head Gaussian splats rigged to FLAME model from multi-view videos captured in a studio environment. *INSTA*[91] employs a multi-resolution hash grid representation [42] for 3D head reconstruction. *FlashAvatar* [75] attaches a uniform 3D Gaussian field in the UV space of the FLAME mesh. Both INSTA and FlashAvatar are monocular-based methods.

5.1. Head Avatar Reconstruction

NeRSemble. As shown in Fig. 4, front-facing monocular videos lack sufficient side-face information. Existing methods can only reconstruct observed regions and leave unobserved areas unconstrained. This often leads to artifacts in extreme hold-out views. In contrast, our approach leverages multi-view diffusion priors to constrain novel views, effectively completing missing regions and enhancing photorealism, while preserving identity and appearance consistency. In Tab. 1, our method surpasses all baselines across metrics, with notable gains of 1.69dB in PSNR and a 5.34% increase in SSIM for novel view synthesis.

Monocular Videos. We also provide the comparisons on the Monocular Video dataset. Since single-view datasets lack ground-truth novel views, we evaluate animation results by applying expression parameters from hold-out frames. As shown in Tab. 2, our method consistently sur-

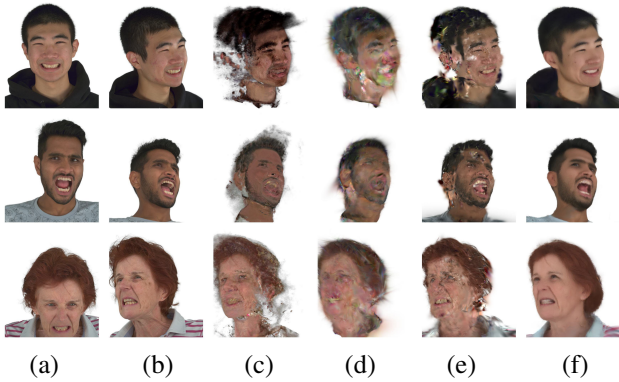


Figure 4. **Novel view synthesis from monocular videos on the NeRsemble dataset.** (a) Input; (b) Ground Truth; (c) INSTA; (d) FlashAvatar; (e) GaussianAvatars; (f) Ours. Compared to state-of-the-art methods, our approach reconstructs unseen side facial regions in the inputs and consistently produces more favorable and consistent renderings from hold-out views.

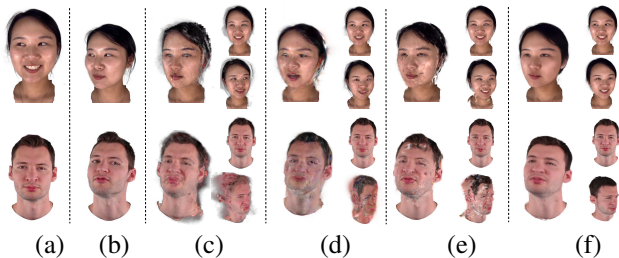


Figure 5. **Head avatar reconstruction from monocular videos captured on commodity devices.** (a) Input; (b) Ground truth of novel expressions; (c) INSTA; (d) FlashAvatar; (e) GaussianAvatars; (f) Ours. For each method, we display the fitting results of the input frame (top right) and novel view renderings of the input frame (bottom right). Given a front-facing sequence with limited head poses, all methods can accurately fit the observed frames. However, without effective priors to constrain unobserved regions, baseline methods struggle to generalize to novel views and poses.

	L1 ↓	LPIPS ↓	PSNR ↑	SSIM ↑
INSTA [91]	0.0407	0.177	21.11	85.04
FlashAvatar [75]	0.0376	0.145	21.13	85.93
GA [48]	0.0263	0.109	22.55	88.61
Ours	0.0228	0.090	23.01	89.93

Table 2. Quantitative comparisons on dynamic avatar reconstruction on **Monocular Video dataset**. Results are obtained by **hold-out expression frames** from six sequences of INSTA and smart-phone capture. Note that **novel view renderings cannot be evaluated** due to the absence of ground truths in single-view captures.

passes others in all metrics. The qualitative results are presented in Fig. 5. While all methods fit well to the input view (top right), baseline methods struggle to generate plausible novel views (bottom right), especially for previously unseen face regions. Baseline methods show limited extrapolation capability, often resulting in artifacts or inconsistencies when animated to novel head poses.

Method	Novel Views			Novel Expressions		
	LPIPS ↓	PSNR ↑	SSIM ↑	LPIPS ↓	PSNR ↑	SSIM ↑
No diffusion	0.207	18.47	82.69	0.129	22.74	88.13
pretrained SD	0.196	16.99	83.47	0.149	21.37	87.81
personalized SD	0.196	16.89	85.98	0.147	21.51	89.52
Ours, w/ SDS	0.178	19.57	84.73	0.136	22.41	87.59
Ours, pose cond.	0.131	19.69	87.63	0.087	23.68	90.37
Ours, w/o latent×2	0.134	21.48	89.53	0.087	25.07	91.75
Ours final	0.118	21.82	89.87	0.079	25.39	92.02

Table 3. **Ablation Studies on different types of diffusion priors.** Results are obtained from the average of six sequences of different subjects from the Nersemble [27] dataset.

5.2. Ablation Studies

We conduct detailed ablation studies to verify the effectiveness of each design in our multi-view head diffusion prior learning. We select six sequences from NeRsemble dataset, including '055 EXP-5', '098 EMO-1', '134 EMO-1', '165 EMO-1', '221 EXP-8', and '417 EMO-4'. The results are presented in Figure 6, and Table 3.

What is the effect of multi-view head diffusion priors?

An alternative is to use pre-trained text-to-image diffusion models Stable Diffusion [52]. Another alternative is to fine-tune Stable Diffusion on RGB frames from the input video, obtaining personalized image diffusion priors. We implement both variants using normal map guidance of ControlNet [84]. In Fig. 6 (d), pre-trained text-to-image priors often produce renderings that deviate from the original identity. In Fig. 6 (e), personalized diffusion priors improve identity preservation but struggle with appearance consistency, as they lack input image information to hallucinate novel views. Our approach learns to jointly generate multiple novel views conditioned on the input image, thus achieving higher realism and view consistency in both identity and appearance.

What is the effect of normal map condition for multi-view diffusion models?

Our multi-view head diffusion models condition on normal maps of FLAME reconstruction, which are pixel-aligned with the target novel-view images. From Fig. 6 (f) reflects that using camera pose conditioning could introduce obvious misalignment errors in synthesizing pseudo-image ground truths, leading to blurred 3D Gaussian renderings.

What is the effect of iteratively denoised images as pseudo-ground-truths?

We can instead use Score Distillation Sampling (SDS) loss to constrain multi-view renderings. As shown in Fig. 6 (g), SDS loss has appearance oversaturation issues in the face region.

What is the effect of latent upsampler module?

Through Fig. 6 (h) vs. (i), we can see that the upsampler module significantly sharpens and enhance facial appearance details.

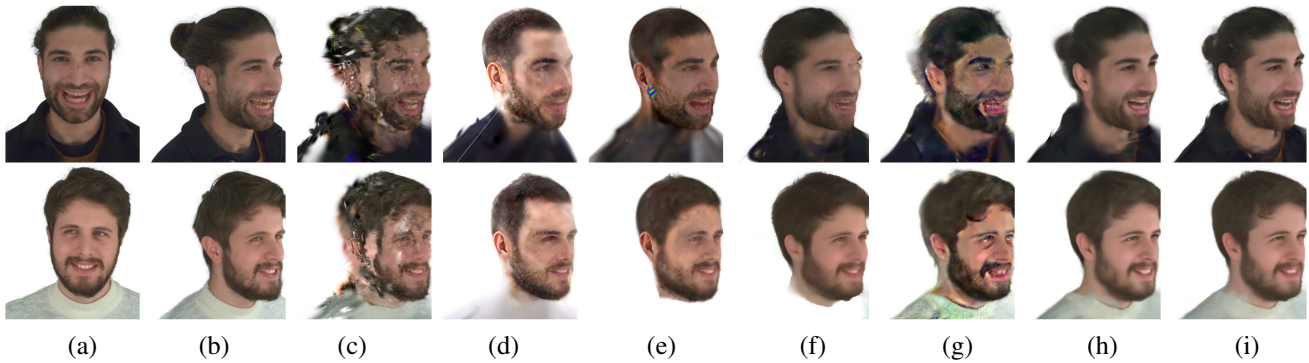


Figure 6. **Ablation Studies on different types of diffusion priors.** (a) Input; (b) Ground truth; Comparisons between method variants of (c) No diffusion; using (d) Pretrained Stable Diffusion; (e) Personalized Stable Diffusion; (f) Pose-conditioned multi-view diffusion; (g) Our multi-view diffusion using Score Distillation Sampling (SDS) loss; (h) Ours without latent upsampler $\times 2$; (i) Ours. Our normal map-conditioned multi-view diffusion priors enable more photo-realistic novel views with identity and appearance consistency, by constraining novel views using pseudo-image ground truths, which are decoded from iteratively denoised latents followed by a latent upsampler.

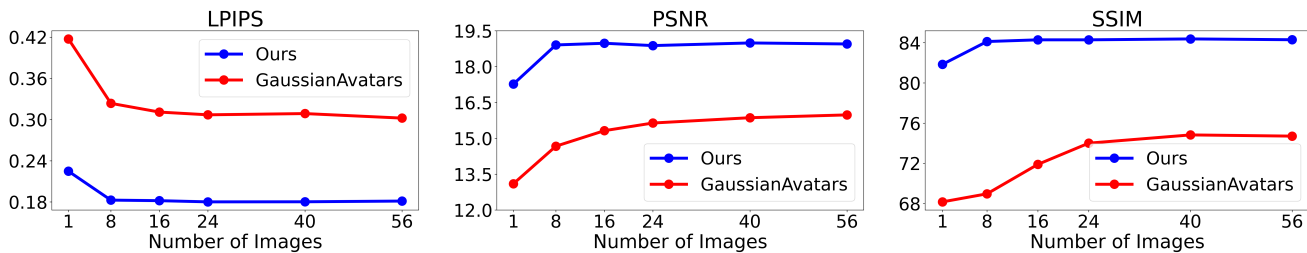


Figure 7. **Robustness analysis to the number of frames in the input monocular video.**

5.3. Robustness Analysis

To demonstrate the robustness of our method with sparse input data, we evaluate reconstruction performance across different frame numbers in the input video. We use the '104 EMO-1' sequence from the NeRSemble dataset, which contains 56 frames in the input. To reduce the frame count, we sample keyframes at uniform intervals. For instance, for an 8-frame input, we select frames at timesteps 0, 7, 14, 21, 28, 35, 42, and 55; for a single-frame input, we use only the 28th frame. As shown in Fig. 15, our method can maintain stable quantitative performance with as few as 8 frames, while GaussianAvatars drops dramatically. This highlights the resilience of our method to limited observations.

5.4. Limitations and Future Work

While our work has shown promising results in dynamic avatar reconstruction from monocular videos captured on studio setups or commodity devices, there are limitations in our current method. First, we do not explicitly separate the material and appearance of heads, which could enable re-lighting applications [24, 56]. Second, optimizing head Gaussians using iteratively updated pseudo ground-truths from diffusion models is time-consuming. We plan to explore real-time 4D avatar reconstruction with feed-forward large reconstruction models [21, 29, 83]. Lastly, the quality of our avatar reconstruction and animation is limited by the expressiveness of current parametric head models,

which lack detailed hair geometry and animation. Future work could extend Gaussian head avatars to incorporate fine-grained hair modeling and animation. [38, 82].

6. Conclusion

In this work, we present a novel method to reconstruct photo-realistic head avatars from monocular videos to push the frontier of avatar fidelity from commodity devices. Due to limited observation and coverage of human heads, Gaussian reconstruction from monocular videos is inherently under-constrained. To address this challenge, we introduce multi-view diffusion priors that jointly constrain photorealism across multiple views rendered from Gaussian splats, while preserving face identity and appearance consistency. We obtain these priors by designing a multi-view head diffusion model, fine-tuned on a multi-view head video dataset to generate novel views from a single image, conditioned on rendered normal maps from FLAME head reconstruction. To prevent appearance over-saturation, we apply an effective diffusion loss using iteratively denoised images as pseudo-ground truths. For finer facial details, we combine a latent upsampler diffusion model with our multi-view diffusion. By reducing data capture requirements for avatar creation, our approach has the potential to unlock new opportunities in immersive VR/AR applications and products.

Acknowledgements

This work was supported by Toyota Motor Europe and Woven by Toyota. This work was also supported by the ERC Starting Grant Scan2CAD (804724). We thank Rundi Wu, Simon Giebenhain, and Lei Li for constructive discussions and Angela Dai for the video voice over.

References

- [1] Ziqian Bai, Feitong Tan, Zeng Huang, Kripasindhu Sarkar, Danhang Tang, Di Qiu, Abhimitra Meka, Ruofei Du, Mingsong Dou, Sergio Orts-Escolano, et al. Learning personalized high quality volumetric head avatars from monocular rgb videos. In *Proceedings of the IEEE/CVF Conference on Computer Vision and Pattern Recognition*, pages 16890–16900, 2023. 1, 2
- [2] Jonathan T Barron, Ben Mildenhall, Matthew Tancik, Peter Hedman, Ricardo Martin-Brualla, and Pratul P Srinivasan. Mip-nerf: A multiscale representation for anti-aliasing neural radiance fields. In *Proceedings of the IEEE/CVF International Conference on Computer Vision*, pages 5855–5864, 2021. 2
- [3] Jonathan T Barron, Ben Mildenhall, Dor Verbin, Pratul P Srinivasan, and Peter Hedman. Mip-nerf 360: Unbounded anti-aliased neural radiance fields. In *Proceedings of the IEEE/CVF Conference on Computer Vision and Pattern Recognition*, pages 5470–5479, 2022.
- [4] Jonathan T Barron, Ben Mildenhall, Dor Verbin, Pratul P Srinivasan, and Peter Hedman. Zip-nerf: Anti-aliased grid-based neural radiance fields. In *Proceedings of the IEEE/CVF International Conference on Computer Vision*, pages 19697–19705, 2023. 2
- [5] Volker Blanz and Thomas Vetter. A morphable model for the synthesis of 3d faces. In *Seminal Graphics Papers: Pushing the Boundaries, Volume 2*, pages 157–164, 2023. 2
- [6] Yukang Cao, Yan-Pei Cao, Kai Han, Ying Shan, and Kwan-Yee K Wong. Dreamavatar: Text-and-shape guided 3d human avatar generation via diffusion models. *arXiv preprint arXiv:2304.00916*, 2023. 3
- [7] Anpei Chen, Zexiang Xu, Andreas Geiger, Jingyi Yu, and Hao Su. Tensorf: Tensorial radiance fields. In *European Conference on Computer Vision*, pages 333–350. Springer, 2022. 2
- [8] Yufan Chen, Lizhen Wang, Qijing Li, Hongjiang Xiao, Shengping Zhang, Hongxun Yao, and Yebin Liu. Monogaussianavatar: Monocular gaussian point-based head avatar. In *ACM SIGGRAPH 2024 Conference Papers*, pages 1–9, 2024. 1
- [9] Yujin Chen, Yinyu Nie, Benjamin Ummenhofer, Reiner Birkel, Michael Paulitsch, Matthias Müller, and Matthias Nießner. Mesh2nerf: Direct mesh supervision for neural radiance field representation and generation. In *European Conference on Computer Vision*, pages 173–191. Springer, 2025. 2
- [10] Matt Deitke, Dustin Schwenk, Jordi Salvador, Luca Weihs, Oscar Michel, Eli VanderBilt, Ludwig Schmidt, Kiana Ehsani, Aniruddha Kembhavi, and Ali Farhadi. Objaverse: A universe of annotated 3d objects. In *Proceedings of the IEEE/CVF Conference on Computer Vision and Pattern Recognition*, pages 13142–13153, 2023. 3
- [11] Matt Deitke, Ruoshi Liu, Matthew Wallingford, Huong Ngo, Oscar Michel, Aditya Kusupati, Alan Fan, Christian Laforte, Vikram Voleti, Samir Yitzhak Gadre, et al. Objaverse-xl: A universe of 10m+ 3d objects. *Advances in Neural Information Processing Systems*, 36, 2024. 3
- [12] Yao Feng, Haiwen Feng, Michael J Black, and Timo Bolkart. Learning an animatable detailed 3d face model from in-the-wild images. *ACM Transactions on Graphics (ToG)*, 40(4): 1–13, 2021. 2
- [13] Sara Fridovich-Keil, Alex Yu, Matthew Tancik, Qinhong Chen, Benjamin Recht, and Angjoo Kanazawa. Plenoxels: Radiance fields without neural networks. In *Proceedings of the IEEE/CVF Conference on Computer Vision and Pattern Recognition*, pages 5501–5510, 2022. 2
- [14] Guy Gafni, Justus Thies, Michael Zollhofer, and Matthias Nießner. Dynamic neural radiance fields for monocular 4d facial avatar reconstruction. In *Proceedings of the IEEE/CVF Conference on Computer Vision and Pattern Recognition*, pages 8649–8658, 2021. 1, 2
- [15] Ruiqi Gao, Aleksander Holynski, Philipp Henzler, Arthur Brussee, Ricardo Martin-Brualla, Pratul Srinivasan, Jonathan T Barron, and Ben Poole. Cat3d: Create anything in 3d with multi-view diffusion models. *arXiv preprint arXiv:2405.10314*, 2024. 3, 4
- [16] Simon Giebenhain, Tobias Kirschstein, Markos Georgopoulos, Martin Rünz, Lourdes Agapito, and Matthias Nießner. Learning neural parametric head models. In *Proceedings of the IEEE/CVF Conference on Computer Vision and Pattern Recognition*, pages 21003–21012, 2023. 1, 2
- [17] Simon Giebenhain, Tobias Kirschstein, Martin Rünz, Lourdes Agapito, and Matthias Nießner. Npga: Neural parametric gaussian avatars. *arXiv preprint arXiv:2405.19331*, 2024. 1
- [18] Philip-William Grassal, Malte Prinzler, Titus Leistner, Carsten Rother, Matthias Nießner, and Justus Thies. Neural head avatars from monocular rgb videos. In *Proceedings of the IEEE/CVF Conference on Computer Vision and Pattern Recognition*, pages 18653–18664, 2022. 2
- [19] Yudong Guo, Lin Cai, and Juyong Zhang. 3d face from x: Learning face shape from diverse sources. *IEEE Transactions on Image Processing*, 30:3815–3827, 2021. 2
- [20] Xiao Han, Yukang Cao, Kai Han, Xiatian Zhu, Jiankang Deng, Yi-Zhe Song, Tao Xiang, and Kwan-Yee K Wong. Headsculpt: Crafting 3d head avatars with text. *Advances in Neural Information Processing Systems*, 36, 2024. 3
- [21] Yicong Hong, Kai Zhang, Jiuxiang Gu, Sai Bi, Yang Zhou, Difan Liu, Feng Liu, Kalyan Sunkavalli, Trung Bui, and Hao Tan. Lrm: Large reconstruction model for single image to 3d. *arXiv preprint arXiv:2311.04400*, 2023. 8
- [22] Bernhard Kerbl, Georgios Kopanas, Thomas Leimkühler, and George Drettakis. 3d gaussian splatting for real-time radiance field rendering. 2023. 1, 2, 3
- [23] Taras Khakhulin, Vanessa Sklyarova, Victor Lempitsky, and Egor Zakharov. Realistic one-shot mesh-based head avatars.

- In *European Conference on Computer Vision*, pages 345–362. Springer, 2022. 2
- [24] Hoon Kim, Minje Jang, Wonjun Yoon, Jisoo Lee, Donghyun Na, and Sanghyun Woo. Switchlight: Co-design of physics-driven architecture and pre-training framework for human portrait relighting. In *Proceedings of the IEEE/CVF Conference on Computer Vision and Pattern Recognition*, pages 25096–25106, 2024. 8
- [25] Diederik P Kingma. Auto-encoding variational bayes. *arXiv preprint arXiv:1312.6114*, 2013. 4
- [26] Diederik P Kingma and Jimmy Ba. Adam: A method for stochastic optimization. *arXiv preprint arXiv:1412.6980*, 2014. 6
- [27] Tobias Kirschstein, Shenhan Qian, Simon Giebenhain, Tim Walter, and Matthias Nießner. Nersemble: Multi-view radiance field reconstruction of human heads. *ACM Transactions on Graphics (TOG)*, 42(4):1–14, 2023. 2, 6, 7, 13, 14
- [28] Samuli Laine, Janne Hellsten, Tero Karras, Yeongho Seol, Jaakko Lehtinen, and Timo Aila. Modular primitives for high-performance differentiable rendering. *ACM Transactions on Graphics*, 39(6), 2020. 14
- [29] Jiahao Li, Hao Tan, Kai Zhang, Zexiang Xu, Fujun Luan, Yinghao Xu, Yicong Hong, Kalyan Sunkavalli, Greg Shakhnarovich, and Sai Bi. Instant3d: Fast text-to-3d with sparse-view generation and large reconstruction model. *arXiv preprint arXiv:2311.06214*, 2023. 8
- [30] Tianye Li, Timo Bolkart, Michael J Black, Hao Li, and Javier Romero. Learning a model of facial shape and expression from 4d scans. *ACM Trans. Graph.*, 36(6):194–1, 2017. 1, 2, 13, 14
- [31] Chen-Hsuan Lin, Jun Gao, Luming Tang, Towaki Takikawa, Xiaohui Zeng, Xun Huang, Karsten Kreis, Sanja Fidler, Ming-Yu Liu, and Tsung-Yi Lin. Magic3d: High-resolution text-to-3d content creation. In *Proceedings of the IEEE/CVF Conference on Computer Vision and Pattern Recognition*, pages 300–309, 2023. 3
- [32] Shanchuan Lin, Andrey Ryabtsev, Soumyadip Sengupta, Brian L Curless, Steven M Seitz, and Ira Kemelmacher-Shlizerman. Real-time high-resolution background matting. In *Proceedings of the IEEE/CVF Conference on Computer Vision and Pattern Recognition*, pages 8762–8771, 2021. 13
- [33] Shanchuan Lin, Linjie Yang, Imran Saleemi, and Soumyadip Sengupta. Robust high-resolution video matting with temporal guidance, 2021. 13
- [34] Ruoshi Liu, Rundi Wu, Basile Van Hoorick, Pavel Tokmakov, Sergey Zakharov, and Carl Vondrick. Zero-1-to-3: Zero-shot one image to 3d object. In *Proceedings of the IEEE/CVF international conference on computer vision*, pages 9298–9309, 2023. 2
- [35] Yuan Liu, Cheng Lin, Zijiao Zeng, Xiaoxiao Long, Lingjie Liu, Taku Komura, and Wenping Wang. Syncdreamer: Generating multiview-consistent images from a single-view image. *arXiv preprint arXiv:2309.03453*, 2023. 3
- [36] Stephen Lombardi, Tomas Simon, Gabriel Schwartz, Michael Zollhoefer, Yaser Sheikh, and Jason Saragih. Mixture of volumetric primitives for efficient neural rendering. *ACM Transactions on Graphics (ToG)*, 40(4):1–13, 2021. 2
- [37] Xiaoxiao Long, Yuan-Chen Guo, Cheng Lin, Yuan Liu, Zhiyang Dou, Lingjie Liu, Yuexin Ma, Song-Hai Zhang, Marc Habermann, Christian Theobalt, et al. Wonder3d: Single image to 3d using cross-domain diffusion. In *Proceedings of the IEEE/CVF Conference on Computer Vision and Pattern Recognition*, pages 9970–9980, 2024. 3
- [38] Haimin Luo, Min Ouyang, Zijun Zhao, Suyi Jiang, Longwen Zhang, Qixuan Zhang, Wei Yang, Lan Xu, and Jingyi Yu. Gaussianhair: Hair modeling and rendering with light-aware gaussians. *arXiv preprint arXiv:2402.10483*, 2024. 8
- [39] Luke Melas-Kyriazi, Iro Laina, Christian Rupprecht, and Andrea Vedaldi. Realfusion: 360deg reconstruction of any object from a single image. In *Proceedings of the IEEE/CVF conference on computer vision and pattern recognition*, pages 8446–8455, 2023. 3
- [40] Luke Melas-Kyriazi, Iro Laina, Christian Rupprecht, Natalia Neverova, Andrea Vedaldi, Oran Gafni, and Filippos Kokkinos. Im-3d: Iterative multiview diffusion and reconstruction for high-quality 3d generation. *arXiv preprint arXiv:2402.08682*, 2024. 3
- [41] Ben Mildenhall, Pratul P Srinivasan, Matthew Tancik, Jonathan T Barron, Ravi Ramamoorthi, and Ren Ng. Nerf: Representing scenes as neural radiance fields for view synthesis. *Communications of the ACM*, 65(1):99–106, 2021. 1, 2
- [42] Thomas Müller, Alex Evans, Christoph Schied, and Alexander Keller. Instant neural graphics primitives with a multiresolution hash encoding. *ACM transactions on graphics (TOG)*, 41(4):1–15, 2022. 1, 2, 6
- [43] Michael Niemeyer, Lars Mescheder, Michael Oechsle, and Andreas Geiger. Occupancy flow: 4d reconstruction by learning particle dynamics. In *Proceedings of the IEEE/CVF international conference on computer vision*, pages 5379–5389, 2019. 2
- [44] Jeong Joon Park, Peter Florence, Julian Straub, Richard Newcombe, and Steven Lovegrove. DeepSDF: Learning continuous signed distance functions for shape representation. In *Proceedings of the IEEE/CVF conference on computer vision and pattern recognition*, pages 165–174, 2019. 2
- [45] Ben Poole, Ajay Jain, Jonathan T Barron, and Ben Mildenhall. Dreamfusion: Text-to-3d using 2d diffusion. *arXiv preprint arXiv:2209.14988*, 2022. 2, 3, 5
- [46] Guocheng Qian, Jinjie Mai, Abdullah Hamdi, Jian Ren, Aliaksandr Siarohin, Bing Li, Hsin-Ying Lee, Ivan Skokhodov, Peter Wonka, Sergey Tulyakov, et al. Magic123: One image to high-quality 3d object generation using both 2d and 3d diffusion priors. *arXiv preprint arXiv:2306.17843*, 2023. 3
- [47] Shenhan Qian. Versatile head alignment with adaptive appearance priors. 2024. 2, 6, 13, 14
- [48] Shenhan Qian, Tobias Kirschstein, Liam Schoneveld, Davide Davoli, Simon Giebenhain, and Matthias Nießner. Gaussianavatars: Photorealistic head avatars with rigged 3d gaussians. *arXiv preprint arXiv:2312.02069*, 2023. 1, 2, 3, 6, 7, 13, 14, 18
- [49] Alec Radford, Jong Wook Kim, Chris Hallacy, Aditya Ramesh, Gabriel Goh, Sandhini Agarwal, Girish Sastry,

- Amanda Askeell, Pamela Mishkin, Jack Clark, et al. Learning transferable visual models from natural language supervision. In *International conference on machine learning*, pages 8748–8763. PMLR, 2021. 2
- [50] Amit Raj, Srinivas Kaza, Ben Poole, Michael Niemeyer, Nataniel Ruiz, Ben Mildenhall, Shiran Zada, Kfir Aberman, Michael Rubinstein, Jonathan Barron, et al. Dreambooth3d: Subject-driven text-to-3d generation. In *Proceedings of the IEEE/CVF International Conference on Computer Vision*, pages 2349–2359, 2023. 3
- [51] Aditya Ramesh, Prafulla Dhariwal, Alex Nichol, Casey Chu, and Mark Chen. Hierarchical text-conditional image generation with clip latents. *arXiv preprint arXiv:2204.06125*, 1(2):3, 2022. 3
- [52] Robin Rombach, Andreas Blattmann, Dominik Lorenz, Patrick Esser, and Björn Ommer. High-resolution image synthesis with latent diffusion models, 2021. 3, 6, 7
- [53] Olaf Ronneberger, Philipp Fischer, and Thomas Brox. U-net: Convolutional networks for biomedical image segmentation. In *Medical image computing and computer-assisted intervention—MICCAI 2015: 18th international conference, Munich, Germany, October 5-9, 2015, proceedings, part III 18*, pages 234–241. Springer, 2015. 4, 14
- [54] Nataniel Ruiz, Yuanzhen Li, Varun Jampani, Yael Pritch, Michael Rubinstein, and Kfir Aberman. Dreambooth: Fine tuning text-to-image diffusion models for subject-driven generation. In *Proceedings of the IEEE/CVF Conference on Computer Vision and Pattern Recognition*, pages 22500–22510, 2023. 4
- [55] Chitwan Saharia, William Chan, Saurabh Saxena, Lala Li, Jay Whang, Emily L Denton, Kamyar Ghasemipour, Raphael Gontijo Lopes, Burcu Karagol Ayan, Tim Salimans, et al. Photorealistic text-to-image diffusion models with deep language understanding. *Advances in neural information processing systems*, 35:36479–36494, 2022. 3
- [56] Shunsuke Saito, Gabriel Schwartz, Tomas Simon, Junxuan Li, and Giljoo Nam. Relightable gaussian codec avatars. In *Proceedings of the IEEE/CVF Conference on Computer Vision and Pattern Recognition*, pages 130–141, 2024. 8
- [57] Zhijing Shao, Zhaolong Wang, Zhuang Li, Duotun Wang, Xiangru Lin, Yu Zhang, Mingming Fan, and Zeyu Wang. Splattingavatar: Realistic real-time human avatars with mesh-embedded gaussian splatting. In *Proceedings of the IEEE/CVF Conference on Computer Vision and Pattern Recognition*, pages 1606–1616, 2024. 1, 2
- [58] Ruoxi Shi, Hansheng Chen, Zhuoyang Zhang, Minghua Liu, Chao Xu, Xinyue Wei, Linghao Chen, Chong Zeng, and Hao Su. Zero123++: a single image to consistent multi-view diffusion base model. *arXiv preprint arXiv:2310.15110*, 2023. 3
- [59] Yichun Shi, Peng Wang, Jianglong Ye, Mai Long, Kejie Li, and Xiao Yang. Mvdream: Multi-view diffusion for 3d generation. *arXiv preprint arXiv:2308.16512*, 2023. 2, 3, 4
- [60] Jiaming Song, Chenlin Meng, and Stefano Ermon. Denoising diffusion implicit models. *arXiv preprint arXiv:2010.02502*, 2020. 5
- [61] Jiapeng Tang, Dan Xu, Kui Jia, and Lei Zhang. Learning parallel dense correspondence from spatio-temporal descriptors for efficient and robust 4d reconstruction. In *Proceedings of the IEEE/CVF Conference on Computer Vision and Pattern Recognition*, pages 6022–6031, 2021. 2
- [62] Jiapeng Tang, Lev Markhasin, Bi Wang, Justus Thies, and Matthias Nießner. Neural shape deformation priors. *Advances in Neural Information Processing Systems*, 35: 17117–17132, 2022. 2
- [63] Jiaxiang Tang, Jiawei Ren, Hang Zhou, Ziwei Liu, and Gang Zeng. Dreamgaussian: Generative gaussian splatting for efficient 3d content creation. *arXiv preprint arXiv:2309.16653*, 2023. 3
- [64] Jiapeng Tang, Angela Dai, Yinyu Nie, Lev Markhasin, Justus Thies, and Matthias Nießner. Dphms: Diffusion parametric head models for depth-based tracking. In *Proceedings of the IEEE/CVF Conference on Computer Vision and Pattern Recognition*, pages 1111–1122, 2024. 1, 2
- [65] Shitao Tang, Fuyang Zhang, Jiacheng Chen, Peng Wang, and Yasutaka Furukawa. Mvdifffusion: Enabling holistic multi-view image generation with correspondence-aware diffusion. *arXiv*, 2023. 3
- [66] Kartik Teotia, Xingang Pan, Hyeonwoo Kim, Pablo Garrido, Mohamed Elgharib, Christian Theobalt, et al. Hq3davatar: High quality controllable 3d head avatar. *arXiv preprint arXiv:2303.14471*, 2023. 2
- [67] Justus Thies, Michael Zollhofer, Marc Stamminger, Christian Theobalt, and Matthias Nießner. Face2face: Real-time face capture and reenactment of rgb videos. In *Proceedings of the IEEE conference on computer vision and pattern recognition*, pages 2387–2395, 2016. 2
- [68] Luan Tran and Xiaoming Liu. Nonlinear 3d face morphable model. In *Proceedings of the IEEE conference on computer vision and pattern recognition*, pages 7346–7355, 2018. 2
- [69] A Vaswani. Attention is all you need. *Advances in Neural Information Processing Systems*, 2017. 4, 14
- [70] Daniel Vlasic, Matthew Brand, Hanspeter Pfister, and Jovan Popovic. Face transfer with multilinear models. In *ACM SIGGRAPH 2006 Courses*, pages 24–es. 2006. 2
- [71] Peng Wang and Yichun Shi. Imagedream: Image-prompt multi-view diffusion for 3d generation. *arXiv preprint arXiv:2312.02201*, 2023. 2, 3, 4, 6
- [72] Zhengyi Wang, Cheng Lu, Yikai Wang, Fan Bao, Chongxuan Li, Hang Su, and Jun Zhu. Prolificdreamer: High-fidelity and diverse text-to-3d generation with variational score distillation. *Advances in Neural Information Processing Systems*, 36, 2024. 3
- [73] Daniel Watson, William Chan, Ricardo Martin-Brualla, Jonathan Ho, Andrea Tagliasacchi, and Mohammad Norouzi. Novel view synthesis with diffusion models. *arXiv preprint arXiv:2210.04628*, 2022. 2, 3
- [74] Rundi Wu, Ben Mildenhall, Philipp Henzler, Keunhong Park, Ruiqi Gao, Daniel Watson, Pratul P. Srinivasan, Dor Verbin, Jonathan T. Barron, Ben Poole, and Aleksander Holynski. Reconfusion: 3d reconstruction with diffusion priors. *arXiv*, 2023. 3, 5
- [75] Jun Xiang, Xuan Gao, Yudong Guo, and Juyong Zhang. Flashavatar: High-fidelity digital avatar rendering at 300fps. *arXiv preprint arXiv:2312.02214*, 2023. 1, 2, 6, 7

- [76] Yuelang Xu, Benwang Chen, Zhe Li, Hongwen Zhang, Lizhen Wang, Zerong Zheng, and Yebin Liu. Gaussian head avatar: Ultra high-fidelity head avatar via dynamic gaussians. *arXiv preprint arXiv:2312.03029*, 2023. 1, 2
- [77] Yuelang Xu, Lizhen Wang, Xiaochen Zhao, Hongwen Zhang, and Yebin Liu. Avatarmv: Fast 3d head avatar reconstruction using motion-aware neural voxels. In *ACM SIGGRAPH 2023 Conference Proceedings*, pages 1–10, 2023. 1
- [78] Yuelang Xu, Zhaoqi Su, Qingyao Wu, and Yebin Liu. Gphm: Gaussian parametric head model for monocular head avatar reconstruction. 2024. 2
- [79] Yuxuan Xue, Xianghui Xie, Riccardo Marin, and Gerard Pons-Moll. Human 3diffusion: Realistic avatar creation via explicit 3d consistent diffusion models. *arXiv preprint arXiv:2406.08475*, 2024. 3, 4
- [80] Changqian Yu, Jingbo Wang, Chao Peng, Changxin Gao, Gang Yu, and Nong Sang. Bisenet: Bilateral segmentation network for real-time semantic segmentation. In *Proceedings of the European conference on computer vision (ECCV)*, pages 325–341, 2018. 13
- [81] Xin Yu, Yuan-Chen Guo, Yangguang Li, Ding Liang, Song-Hai Zhang, and Xiaojuan Qi. Text-to-3d with classifier score distillation. *arXiv preprint arXiv:2310.19415*, 2023. 3
- [82] Egor Zakharov, Vanessa Sklyarova, Michael Black, Giljoo Nam, Justus Thies, and Otmar Hilliges. Human hair reconstruction with strand-aligned 3d gaussians. In *European Conference on Computer Vision*, pages 409–425. Springer, 2025. 8
- [83] Kai Zhang, Sai Bi, Hao Tan, Yuanbo Xiangli, Nanxuan Zhao, Kalyan Sunkavalli, and Zexiang Xu. Gs-irm: Large reconstruction model for 3d gaussian splatting. In *European Conference on Computer Vision*, pages 1–19. Springer, 2025. 8
- [84] Lvmin Zhang, Anyi Rao, and Maneesh Agrawala. Adding conditional control to text-to-image diffusion models. In *Proceedings of the IEEE/CVF International Conference on Computer Vision*, pages 3836–3847, 2023. 7
- [85] Mingwu Zheng, Hongyu Yang, Di Huang, and Liming Chen. Imface: A nonlinear 3d morphable face model with implicit neural representations. In *Proceedings of the IEEE/CVF Conference on Computer Vision and Pattern Recognition*, pages 20343–20352, 2022. 2
- [86] Xiaozheng Zheng, Chao Wen, Zhaohu Li, Weiyi Zhang, Zhuo Su, Xu Chang, Yang Zhao, Zheng Lv, Xiaoyuan Zhang, Yongjie Zhang, et al. Headgap: Few-shot 3d head avatar via generalizable gaussian priors. *arXiv preprint arXiv:2408.06019*, 2024. 2
- [87] Yufeng Zheng, Victoria Fernández Abrevaya, Marcel C Bühler, Xu Chen, Michael J Black, and Otmar Hilliges. Im avatar: Implicit morphable head avatars from videos. In *Proceedings of the IEEE/CVF Conference on Computer Vision and Pattern Recognition*, pages 13545–13555, 2022. 1, 2
- [88] Yufeng Zheng, Wang Yifan, Gordon Wetzstein, Michael J Black, and Otmar Hilliges. Pointavatar: Deformable point-based head avatars from videos. In *Proceedings of the IEEE/CVF conference on computer vision and pattern recognition*, pages 21057–21067, 2023. 1, 2
- [89] Zhenglin Zhou, Huaxia Li, Hong Liu, Nanyang Wang, Gang Yu, and Rongrong Ji. Star loss: Reducing semantic ambiguity in facial landmark detection. In *Proceedings of the IEEE/CVF Conference on Computer Vision and Pattern Recognition (CVPR)*, pages 15475–15484, 2023. 14
- [90] Zhenglin Zhou, Fan Ma, Hehe Fan, and Yi Yang. Headstudio: Text to animatable head avatars with 3d gaussian splatting. *arXiv preprint arXiv:2402.06149*, 2024. 3
- [91] Wojciech Zielonka, Timo Bolkart, and Justus Thies. Instant volumetric head avatars. In *Proceedings of the IEEE/CVF Conference on Computer Vision and Pattern Recognition*, pages 4574–4584, 2023. 1, 2, 6, 7
- [92] Qi Zuo, Xiaodong Gu, Lingteng Qiu, Yuan Dong, Zhengyi Zhao, Weihao Yuan, Rui Peng, Siyu Zhu, Zilong Dong, Liefeng Bo, et al. Videomv: Consistent multi-view generation based on large video generative model. *arXiv preprint arXiv:2403.12010*, 2024. 3

Appendix

In this supplementary material, we provide additional information about the dataset in Sec. A. Subsequently, we present more detailed explanations about method implementations in Sec. B, including parametric head tracking and multi-view head diffusion. Following that, we showcase the results of our multi-view head diffusion results in Sec. C. Next, we provide additional comparisons in Sec. D, including novel view synthesis, self-/cross-reenactment, and robustness analysis. Finally, we discuss the ethical considerations and potential negative impacts in Section E.

A. Dataset

Smartphone Video Capture. We capture monocular video sequences using an iPhone 14 Pro. The subject is seated in a chair, and the room lights are turned on during the recording, providing adequate illumination. The duration of the recording is about 10-15 seconds, at 30 frames per second. The image resolution is 1280×720 .

Data preprocessing. To simplify the optimization process for animatable Gaussian splats, we integrate two preprocessing steps on raw images extracted from monocular videos. Firstly, we leverage the image matting techniques proposed in [32, 33] to remove the background. More specifically, we use [33] for our smartphone video capture, while we adopt [32] for the NeRSemble [27] dataset, where the initial background image is provided. Secondly, we utilize face segmentation maps acquired from BiSeNet [80] to isolate and crop out the torso portion, thus concentrating solely on head reconstruction. An example of our image preprocessing pipeline is illustrated in Fig. 8.

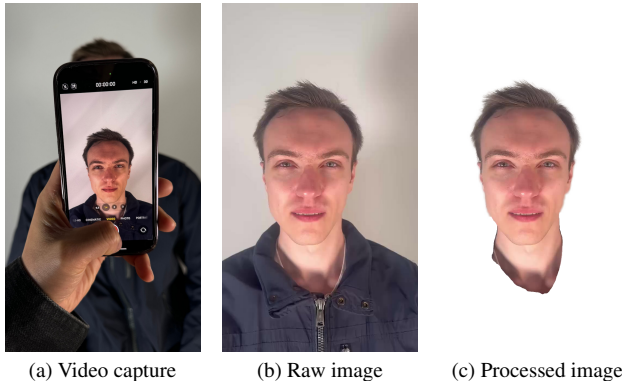


Figure 8. **Data capture and processing of monocular videos from smartphones.** We capture a short video using an iPhone 14 Pro. From the raw images, we remove the background using image matting techniques and segment out the torso to focus on the head region.

Train-Test Split. In the NeRSemble dataset, we use monocular videos from the 8-th camera as the input, only

#Sequence Names	#timesteps \times #cams		
	Train	Novel view	Novel expression
017 EXP-5	208×1	208×15	52×5
037 EXP-8	203×1	203×15	50×5
055 EMO-4	105×1	105×15	26×5
074 EXP-5	179×1	179×15	44×5
134 EMO-1	79×1	79×15	19×5
165 EXP-8	189×1	189×15	47×5
221 EXP-5	147×1	147×15	36×5
251 EMO-1	51×1	51×15	12×5
264 EMO-1	75×1	75×15	18×5
304 EMO-1	127×1	127×15	31×5
417 EMO-4	124×1	124×15	31×5
460 EXP-4	124×1	124×15	30×5

Table 4. **Statistics of the train/val/test splits used for NeRSemble sequences.** For each sequence, we use 80% of timesteps for the training and validation datasets. We select the 8th camera (front-facing) for the train split, while all remaining cameras are used for novel-view evaluation (validation set). The novel-expression evaluation is conducted by selecting 5 nearby cameras for the remaining 20% of timesteps (test set).

capturing the head from the front view. we evaluate head avatar reconstruction and animation quality in two settings: 1) *novel view synthesis*: driving a reconstructed avatar with seen head poses and expressions during training, and rendering it from 15 hold-out viewpoints. 2) *novel expression synthesis*: driving a reconstructed avatar with unseen head poses and expressions during training, rendering it from 5 nearby hold-out views, *i.e.* cameras 6–10. In Tab. 4, we provide detailed statistics about the used sequences in NeRSemble and train/val/test split.

The statistics of the monocular video data are summarized in Tab. 5. Since monocular videos captured on commodity devices lack corresponding ground truths for novel view renderings, we only evaluate avatar animation performance in the quantitative comparisons, by applying pose and expression parameters from unseen frames during training.

B. Implementations

B.1. Monocular Head Tracking

We track the FLAME [30] parameters using the VHAP-tracker [47] proposed in [48]. Given a monocular video we optimize both shared parameters (shape, albedo map, diffuse light) and per-timestep parameters (pose, translation, expression). The tracking algorithm is divided into three stages: (i) initialization stage; (ii) sequential optimization stage; (iii) global optimization stage. The tracking process

#Sequence Names	#timesteps	
	Train	Test
wojteck-1	760	2678
person0004	450	1050
subject1	229	48
subject2	312	83
subject3	139	34
subject4	440	154

Table 5. **Statistics of the train/test splits used for the Monocular Video dataset.** To effectively evaluate the ability of our method to represent unseen regions of the head, we select training frames with limited head rotation. The remaining frames, which contain unseen poses and expressions, are used as the test set.

begins with an initialization stage, performed on the first frame of the video, which sets up all the aforementioned parameters. Following this, a sequential optimization stage is applied to each successive frame of the video. In this stage, the parameters of each frame are optimized for 50 iterations, using the previous timestep as initialization. Finally, the tracking parameters are refined through a global optimization stage, where a random frame is sampled at each iteration, for a total of 30 epochs.

The tracking is performed by minimizing a combination of multiple energy terms: (i) a photometric energy term, computed between the rendered image and the ground-truth one; (ii) a landmarks energy term, which computes the distance between the projected 2D FLAME [30] landmarks and the 2D landmarks predicted by an off-the-shelf detector [89]; (iii) temporal energy terms, applied on the per-timestep parameters, which ensure smoothness over time; (iv) regularization energy terms, applied on all FLAME [30] parameters. We revised the loss weights for the smoothness terms as: $\lambda_{smooth,transl} = 3e4$, $\lambda_{smooth,rot} = 3e3$, $\lambda_{smooth,jaw} = 4.0$, $\lambda_{smooth,eyes} = 1.0$, $\lambda_{smooth,expr} = 0.5$. For all the remaining hyper-parameters we refer to the original work [47].

We use NVDiffRast [28] as the differentiable mesh renderer and the FLAME 2023 version [30] with the additional 168 triangles to represent the teeth, as proposed by [48].

B.2. Multi-view Latent Head Diffusion

In Fig. 10, we show the network architecture details of our multi-view head latent diffusion. The denoiser network is based on a 2D U-Net [53] with attention blocks [69]. The U-Net comprises four Down Blocks, one Middle Block, and four Up Blocks. Each Down Block contains a Residual block, a 3D Attention block, and a Downsampling layer. The Middle Block is composed of a Residual block and a

3D Attention block. The Up Block mirrors the Down blocks but with Upsampling layers.

C. Generation Results of Multi-view Head Diffusion

In Fig. 9, we showcase the sampling results from our multi-view head diffusion model. The model generates four view-consistent images from a single input image while effectively preserving facial identity and appearance. This demonstrates the model’s capability to synthesize coherent and identity-preserving novel views.

D. Additional Comparisons

D.1. Dynamic Head Avatar Reconstruction

In Fig. 11 and Fig. 12, we provide additional qualitative comparisons on dynamic head avatar reconstruction from monocular videos sampled from NerSemble dataset [27].

D.2. Self- & Cross-Reenactment

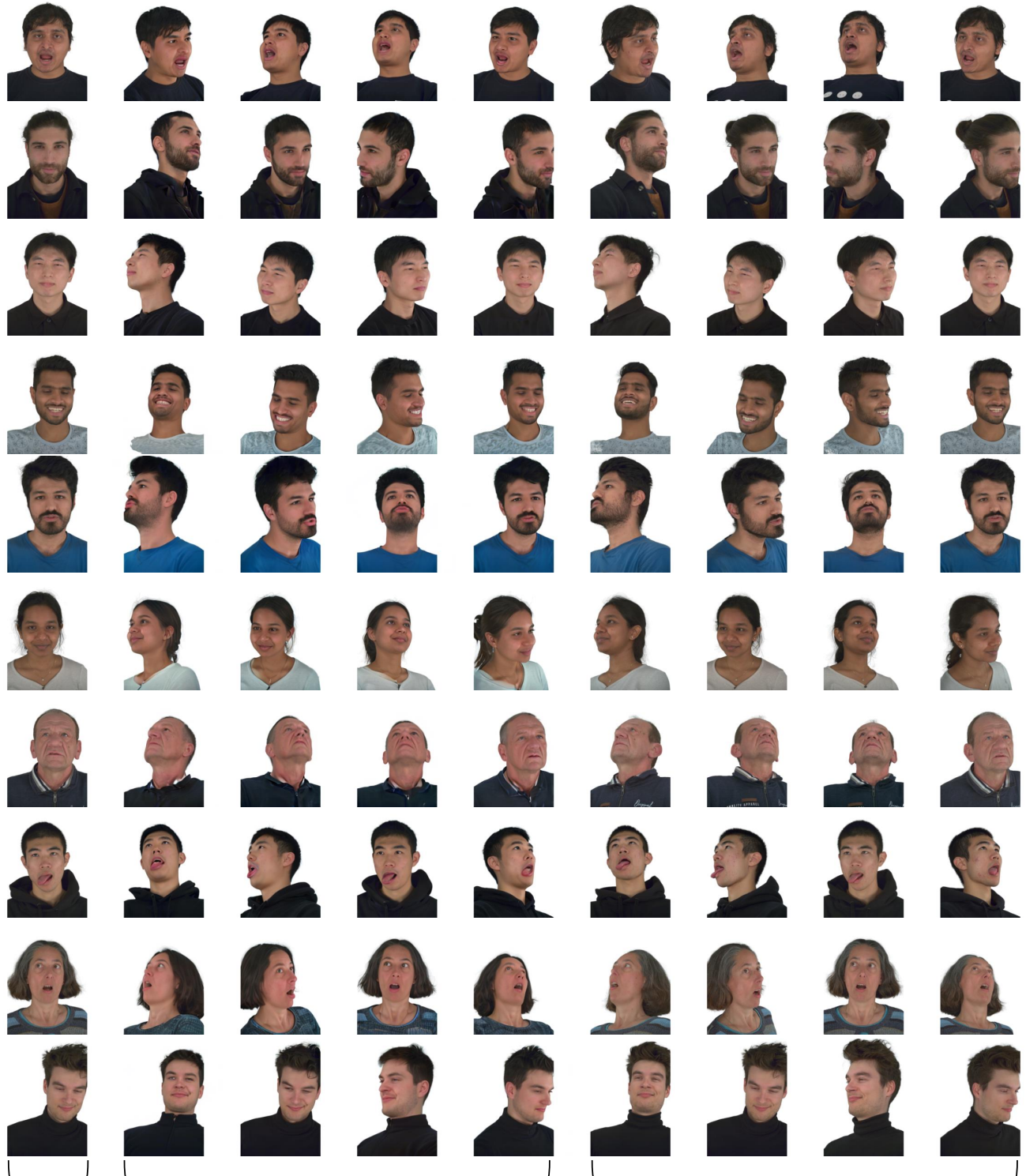
We show the self and cross reenactment results of our method and Gaussian Avatars in Fig. 13 and 14.

D.3. Robustness Analysis

In Fig. 15, we present qualitative results from a robustness analysis conducted with varying numbers of frames in the input monocular videos. Our approach consistently achieves photorealistic novel view rendering across various sequence lengths, even with only 8 frames as input.

E. Ethical Discussion and Negative Impacts

The creation of photorealistic and animatable head avatars from an input video poses several ethical challenges and significant risks related to the possible malevolent usage of this technology. One major concern is the potential for misuse in creating deepfakes, which are highly realistic but fake videos that can be used to spread misinformation, manipulate public opinion, or damage reputations. Additionally, this technology can lead to privacy violations, as individuals’ likenesses can be replicated without their consent, leading to unauthorized use in various contexts. There is also the risk of identity theft, where malicious actors could use these avatars to impersonate others for fraudulent activities. Moreover, the psychological impact on individuals who see their digital likeness used inappropriately can be profound, causing distress and harm. Our commitment is to promote the responsible and ethical use of this technology, and we are firmly against any malicious usage that aims to harm individuals or communities.



Input

Generation Sample

Ground Truth

Figure 9. **Generation sample results of the multi-view head latent diffusion model.** Given a single image as input, our method can generate identity-preserved, and view-consistent multi-view portrait images.

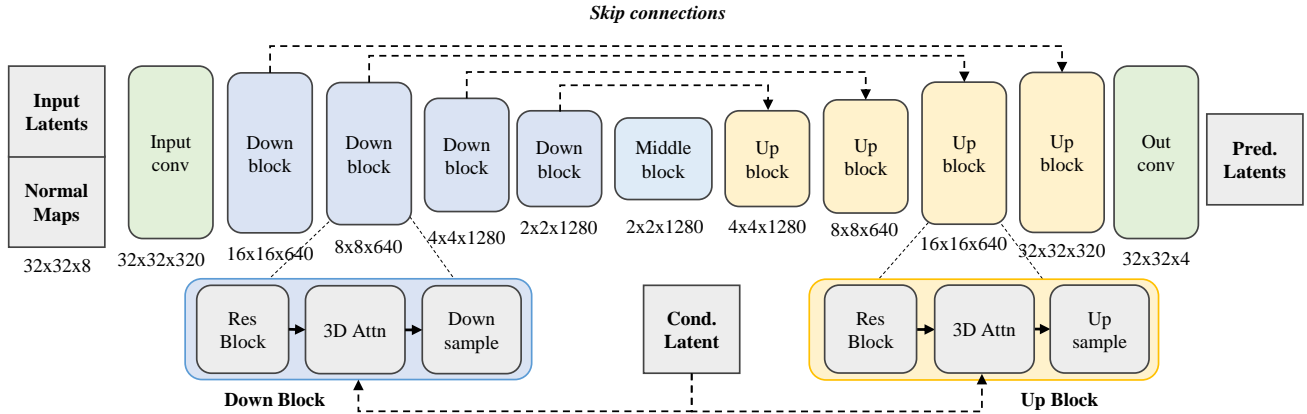


Figure 10. **Network architecture of our multi-view head latent diffusion model.** The denoiser network is built on a 2D U-Net architecture with attention blocks. The input consists of multi-view image latents concatenated with VAE latents of normal maps rendered from the FLAME mesh. The 3D Attention block enforces 3D consistency by applying cross-attention across all views. It also incorporates the input image latent into the denoising process, effectively preserving the identity and appearance details of the input portrait.

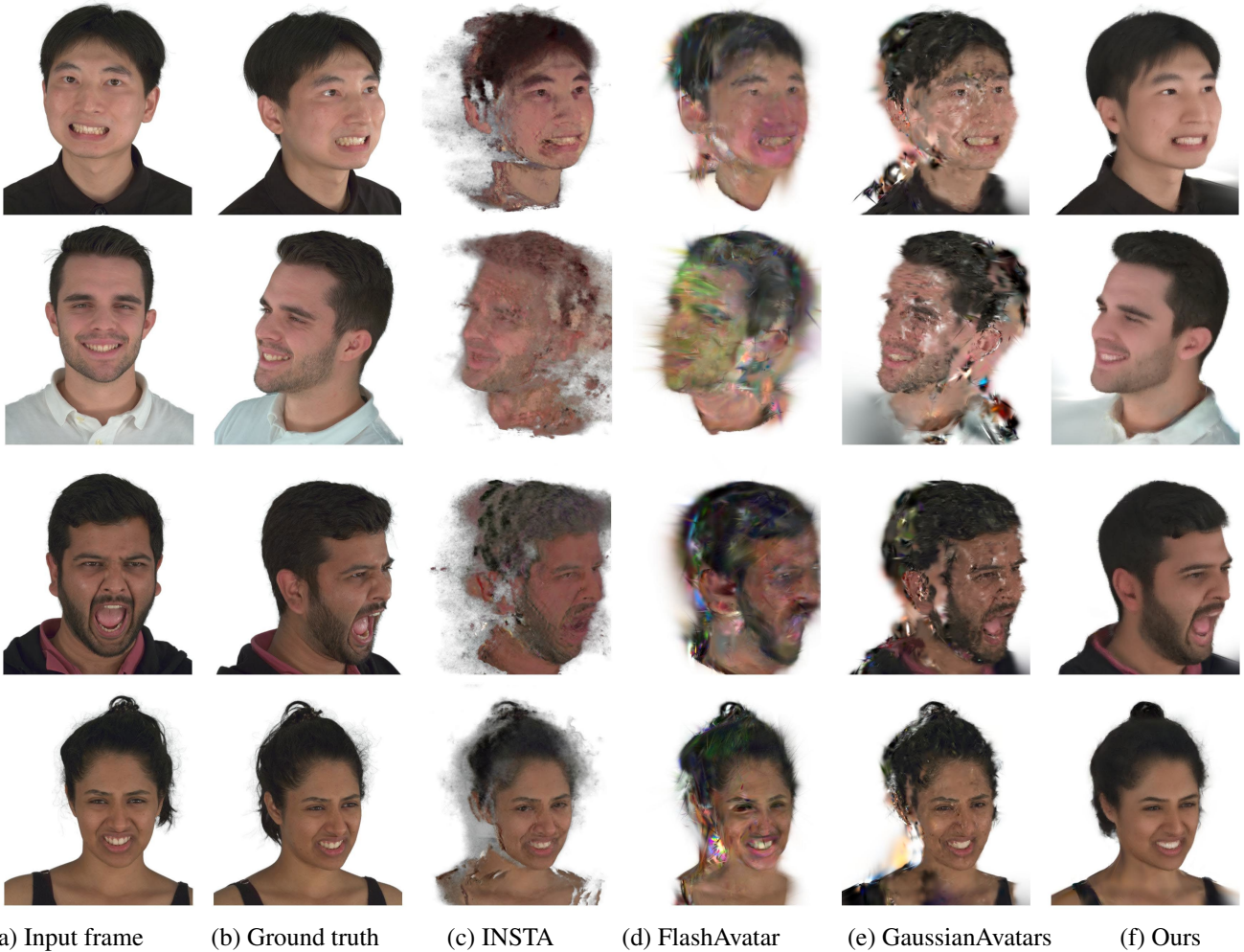


Figure 11. **Additional results on novel view synthesis from monocular videos from the NeRsemble dataset.** Our method demonstrates robust reconstruction of less observed regions, such as side facial areas, and consistently produces more plausible and view-consistent renderings from hold-out views.

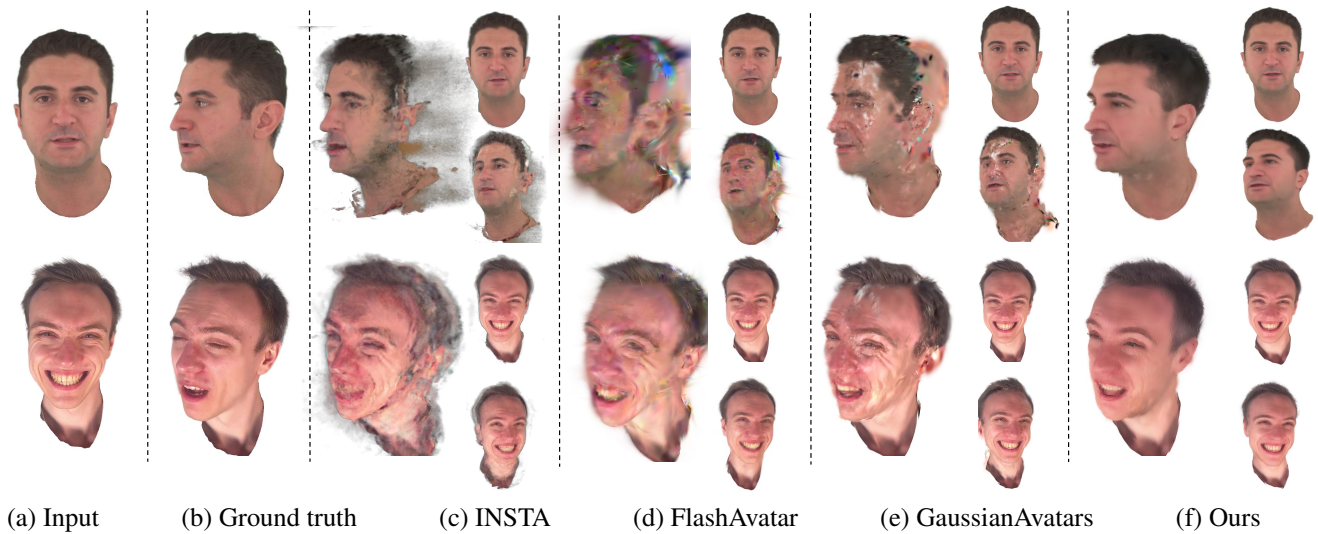


Figure 12. **Additional results of head avatar reconstruction from monocular videos on commodity devices.** We present novel expression animation results using unseen frames from the monocular videos during training. Additionally, we display the fitting results for the input frame (top right) and novel view renderings of the same frame (bottom right). While all methods accurately fit observed frames in front-facing sequences with limited head poses, baseline methods fail to generalize to novel views and poses due to the absence of effective priors for less unobserved regions.

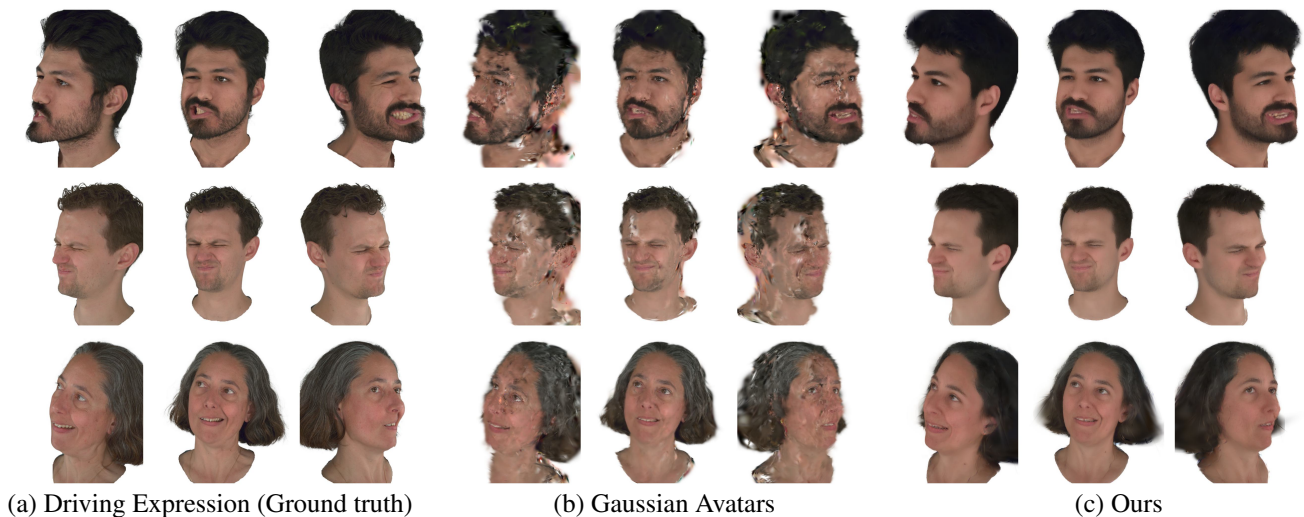


Figure 13. **Self-reenactment from monocular videos on the NeRSemle dataset.** We use the tracked FLAME pose and expressions of a driving sequence to animate the reconstructed Gaussians. We show three novel view renderings for each reenactment result. Our method demonstrates more plausible head animations through more detailed face reconstruction, such as wrinkles, and faithfully produces view-consistent head renderings from different novel viewpoints.

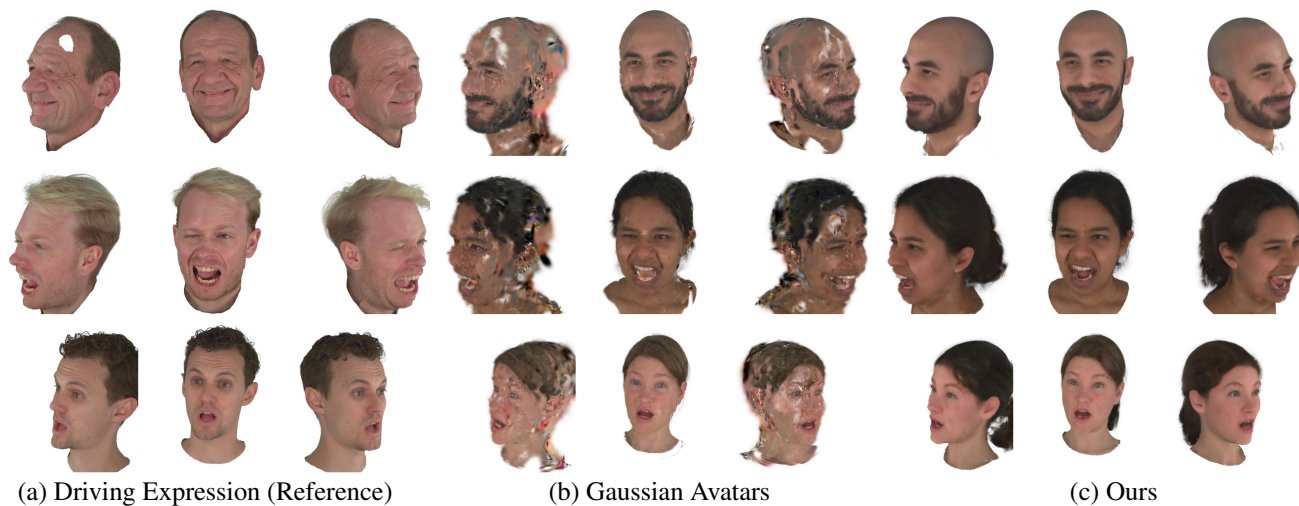


Figure 14. **Cross-reenactment from monocular videos on the Nersemble dataset.** We show three novel view renderings for each reenactment result. Our method outperforms Gaussian Avatars by showcasing more vivid expression transfers and more plausible renderings around the mouth.

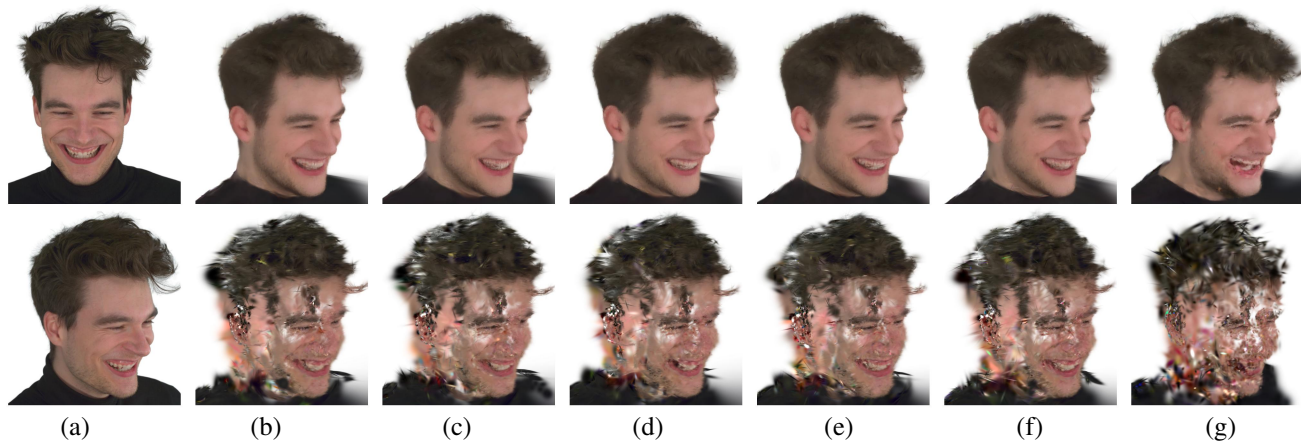


Figure 15. **Robustness analysis to the number of frames in the input monocular video.** (a) Input view (top) & Ground truth (bottom); (b) 56 frames; (c) 40 frames; (d) 24 frames; (e) 16 frames; (f) 8 frames; (g) 1 frame. Compared to GaussianAvatars [48], our method demonstrates robust reconstruction of novel view synthesis even with as few as eight frames, highlighting its robustness to limited observations.